SPHERICAL FUNCTION REGULARIZATION FOR PARALLEL MRI RECONSTRUCTION

Abstract. From the optimization point of view, a difficulty with parallel MRI with simultaneous coil sensitivity estimation is the multiplicative nature of the non-linear forward operator: the image being reconstructed and the coil sensitivities compete against each other, causing the optimization process to be very sensitive to small perturbations. This can, to some extent, be avoided by regularizing the unknown in a suitably "orthogonal" fashion. In this paper, we introduce such a regularization based on spherical function bases. To perform this regularization, we represent efficient recurrence formulas for spherical Bessel functions and associated Legendre functions. Numerically, we study the solution of the model with non-linear ADMM. We perform various numerical simulations to demonstrate the efficacy of the proposed model in parallel MRI reconstruction.

Key words. Parallel MRI, spherical function, regularization, coil sensitivity, ADMM

AMS subject classifications. 65K10, 33C10, 33C55, 68U10, 68W25

1. Introduction. Parallel MR imaging can be formulated as a nonlinear inverse problem with a nonlinear forward operator $\mathfrak{F}$, which maps the proton density u and the coil sensitivities $c = (c_j, c_2, \ldots, c_J)^T$ to the measured k-space data g as

$$\mathfrak{F}(u, c) := \left(P\mathcal{F}(u \cdot c_1), P\mathcal{F}(u \cdot c_2), \ldots, P\mathcal{F}(u \cdot c_J)\right)^T = g. \tag{1}$$

Here P is the binary sub-sampling mask, $\mathcal{F}$ is the discrete 2D Fourier transform, and $g = (g_1, g_2, \ldots, g_J)^T$ the acquired k-space measurements for J receiver coils. As shown in [11, 9], the problem (1) can be solved by the iteratively regularized Gauss-Newton (IRGN) method [2, 7, 6, 8].

Instead of the iteratively regularized IRGN approach, in this paper we will assume that the coil sensitivities can be sparsely represented in a spherical function basis $\{f_l^+\}$. With $c_j = \sum_{l=1}^{L} a_l^{(j)} f_l^+$, we will in the variational model promote sparsity by taking

$$R_c(c) = \alpha R_a(a) \quad \text{for} \quad R_a(a) = \sum_{j=1}^{J} \sum_{l=1}^{L} |a_l^{(j)}|.$$

Therefore, we consider the model

$$\min_{v=(u,a)} \frac{1}{2} \sum_{j=1}^{J} \left\| P\mathcal{F}(G(v))_j - g_j \right\|_2^2 + \alpha_0 R_u(u) + \alpha R_a(a), \tag{2}$$

for an appropriate definition of G that we provide in section 2.

2. The new regularization model and its numerical realization. In order to cast the model (2) in the preconditioned ADMM framework, we define

$$B(v) := \Big(G(v), \nabla u, a\Big),$$

. By analogue, following [3], we extend the preconditioned ADMM to non-linear B as

$$w^{k+1} = \operatorname*{argmin}_v \; F(p^k) + \langle \lambda^k, B(v) - p^k \rangle + \frac{\delta}{2} \left\| B(v) - p^k \right\|^2 + \rho_{k+1}^{-1} \left\| v - w^k \right\|_{Q_v^k}^2, \tag{3a}$$

$$p^{k+1} = \operatorname*{argmin}_q \; F(q) + \langle \lambda^k, B(w^{k+1}) - q \rangle + \frac{\delta}{2} \left\| B(w^{k+1}) - q \right\|^2 + \rho_{k+1}^{-1} \left\| q - p^k \right\|_{Q_q^k}^2, \tag{3b}$$

$$\lambda^{k+1} = \lambda^k + \delta(B(w^{k+1}) - p^{k+1}). \tag{3c}$$

For our specific problem, the minimizations are over $v \in \mathbb{R}^{N^2+J*l_{\max}^{(\tilde{n})}}$, and $q \in \mathbb{R}^{J*N^2+2*N^2+J*l_{\max}^{(\tilde{n})}}$.

Since these functions are smooth,

$$\tilde{F}_1(v) \approx \tilde{F}_1(w^k) + \tilde{F}_1{}'(w^k)(v - w^k), \quad \text{and} \quad \tilde{F}_2(q) \approx \tilde{F}_2(p^k) + \tilde{F}_2{}'(p^k)(v - p^k), \tag{4}$$

where $\tilde{F}_1{}'(w^k)$ and $\tilde{F}_2{}'(p^k)$ are the Fréchet derivative of $\tilde{F}_1$ at w^k and $\tilde{F}_2$ at p^k. Using (4), (3a), and (3b) are replaced by

$$w^{k+1} = \underset{v}{\operatorname{argmin}} \langle \lambda^k, J_q^k v\rangle + \frac{\delta}{2}\left\|J_q^k v - r_v^k\right\|^2 + \rho_{k+1}^{-1}\left\|v - w^k\right\|_{Q_v^k}^2, \tag{5a}$$

$$p^{k+1} = \underset{q}{\operatorname{argmin}}\ F(q) + \langle \lambda^k, J_q^k v\rangle + \frac{\delta}{2}\left\|J_q^k v - r_v^k\right\|^2 + \rho_{k+1}^{-1}\left\|q - p^k\right\|_{Q_q^k}^2, \tag{5b}$$

where still $v \in \mathbb{R}^{N^2+J*l_{\max}^{(\tilde{n})}}$, and $q \in \mathbb{R}^{J*N^2+2*N^2+J*l_{\max}^{(\tilde{n})}}$.

It follows easily from (5a) and (5b)

$$w^{k+1} = w^k - \tau_v^k J_v^{k*}\bar{\lambda}^k, \tag{6}$$

$$p^{k+1} = \left(I + \tau_q^k \partial F\right)^{-1}\left(p^k - \tau_q^k J_q^{k*}\left(\lambda^k + \delta\left(B(w^{k+1}) - p^k\right)\right)\right). \tag{7}$$

Finally, (6), (7) and (3c) yields Algorithm 1 for the solution of (2). Its convergence is studied in [3] based on the results of [12].

Algorithm 1 Linearised preconditioned ADMM for (2)

Initialization w^0, p^0, λ^0 and δ.
Set $\bar{\lambda}^0 = \mu^0$.
while "stopping criterion is not satisfied" **do**
  $J_v^k = \tilde{F}_1{}'(w^k)$
  Choose τ_v^k such that $\tau_v^k \delta < \frac{1}{\|J_v^k\|^2}$
  Compute w^{k+1} by (6)
  Compute J_q^k by $J_q^k = \tilde{F}_2{}'(p^k)$
  Choose τ_q^k such that $\tau_q^k \delta < \frac{1}{\|J_q^k\|^2}$
  Compute p^{k+1} by (7)
  Compute λ^{k+1} by (3c)
  Compute $\bar{\lambda}^{k+1} = 2\lambda^{k+1} - \lambda^k$
end while
Return w^k, p^k, λ^k and $\bar{\lambda}^k$
Output the reconstruction image u^k and the coefficient vector a^k via w^k.

3. Numerical experiments. Our numerical experiments are based on the synthetic brain phantom from [1, 5]. In the numerical simulations, we set the number of coils $J = 8$. For the generation of k-space measurement data g_j, $j = 1, 2, \ldots, J$, we use the approach of [3]. We generate 8 coil sensitivity maps based on a measurement of a water bottle with an 8-channel head coil array. We apply the 25% subsampling mask shown in Figure 1. We evaluate the results of the proposed approach in terms of the peak signal-to-noise (PSNR) and the Structural SIMilarity (SSIM) given in [13]. In the computation of the spherical basis function f_l^+, we use the Larmour frequency $\omega = 42.58$. The conductivity σ and the dielectric permittivity ε are the optimal (σ, ε) for the heterogeneous model in [10] with $\sigma = 0.6, \varepsilon = 50$. The magnetic permeability for water is $\mu = 1.2566 \times 10^{-6}$. We initialize the Algorithm 1 with

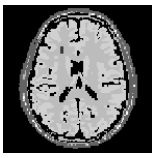

(a) Brain phantom

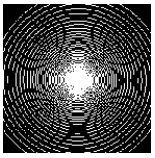

(b) k-space sampling mask

Fig. 1: (a) shows the brain phantom. (b) shows the spiral-shaped 25% k-space sub-sampling mask.

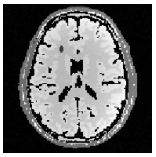

(a) 1200 iterations

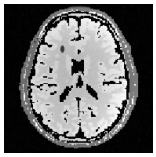

(b) 1500 iterations

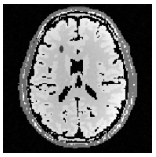

(c) 1800 iterations

Fig. 2: Reconstructed brain slice using (2) and $\tilde{n} = 5$.

$u^0 = 0 \in \mathbb{R}^{N^2}$, $a^0 = (1, \ldots, 1) \in \mathbb{R}^{Jl_{\max}^{(n)}}$, and take as step lengths $\tau_v^k = 1/8$, $\tau_q^k = 23$, and $\delta = 1/24$ and the remaining v^0, λ^0, $\bar{\lambda}^0$ are all also initialized to zero in the two algorithms. For numerical reconstruction corresponding to (1), we use the codes from [3], available from [4]. With $\tilde{n} = 5$, stopping after 1000, 1200, and 1500 iterations, the reconstruction results for the model (2) are shown in Figure 2. The reconstruction results for the model (1) in Figure 3. In Table 1 we report the PNSR and SSIM [13] values. From these results we can observe that the reconstruction quality of the model (2) is much better than the model (1) when iterations are 1000, 1200, and 1500.

4. Conclusions. In this paper, we have established a new model for parallel MRI reconstruction based on sparse regularization of coil sensitivities in spherical basis function bases. We have developed efficient recurrence formulas for the computation of these functions. By numerical reconstructions and comparison between (2) and (1), we think that the reconstruction quality for proposed model (2) is better than the model (1).

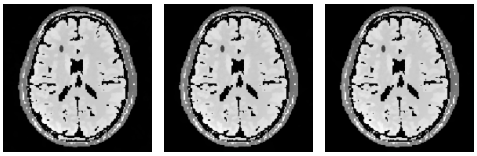

(a) 1200 iterations (b) 1500 iterations (c) 1800 iterations

Fig. 3: Reconstructed brain slice using (1).

Table 1: Reconstruction quality comparison between (2) with $\tilde{n} = 2, 5$ and (1).

Method	stopping itr. k	PSNR(dB)	SSIM
using (2) with $\tilde{n} = 5$	1200	26.0725	0.9997
	1500	25.5883	0.9997
	1800	25.8730	0.9997
using (1)	1200	24.7173	0.9996
	1500	24.1524	0.9996
	1800	23.6702	0.9995

[1] B. Aubert-Broche, A. C. Evans, and L. Collins, *A new improved version of realistic digital brain phantom*, NeuroImage, 32 (2006), pp. 138–145.

[2] A. B. Bakushinsky and M. Y. Kokurin, *Iterative methods for approximate solution of inverse problems*, Mathematics and its Applications, Vol. 577. Springer, 2004.

[3] M. Benning, F. Knoll, C.-B. Schönlieb, and T. Valkonen, *Preconditioned ADMM with nonlinear operator constraint*, in System Modeling and Optimization: 27th IFIP TC 7 Conference, CSMO 2015, Sophia Antipolis, France, June 29–July 3, 2015, Revised Selected Papers, L. Bociu, J.-A. Désidéri, and A. Habbal, eds., Springer International Publishing, 2016, pp. 117–126, https://doi.org/10.1007/978-3-319-55795-3_10.

[4] M. Benning, F. Knoll, C. B. Schönlieb, and T. Valkonen, *Research data supporting: Preconditioned ADMM with nonlinear operator constraint*, 2016, https://doi.org/10.17863/CAM.163.

[5] M. A. Bernstein, K. F. King, and X. J. Zhou, *Handbook of MRI Pulse Sequences*, Elsevier, 2004.

[6] B. Blaschke, A. Neubauer, and O. Scherzer, *On convergence rates for the iteratively regularized gauss-newton method*, IMA J Numer Anal., 17 (1997), pp. 421–436.

[7] H. W. Engl, M. Hanke, and A. Neubauer, *Regularization of inverse problems*, Mathematics and its Applications, Vol. 375. Kluwer Academic Publishers Group, 1996.

[8] T. Hohage, *Logarithmic convergence rates of the iteratively regularized gauss-newton method for an inverse potential and an inverse scattering problem*, Inverse Problems, 13 (1997), pp. 1279–1299.

[9] F. Knoll, C. Clason, M. Uecker, and R. Stollberger, *Improved Reconstruction in Non-cartesian Parallel Imaging by Regularized Nonlinear Inversion*, Proceedings of the 17th Scientific Meeting and Exhibition of ISMRM, Honolulu, HI, 2009.

[10] A. Sbrizzi, H. Hoogduin, J. J. Lagendijk, P. Luijten, and C. A. T. van den Berg, *Robust reconstruction of b_1^+ maps by projection into a spherical functions space*, Magn. Reson. Med., 71 (2014), pp. 394–401.

[11] M. Uecker, T. Hohage, K. T. Block, and J. Frahm, *Image reconstruction by regularized nonlinear inversion-joint estimation of coil sensitivities and image content*, Magn. Reson. Med., 60 (2008), pp. 674–682.

[12] T. Valkonen, *A primal-dual hybrid gradient method for non-linear operators with applications to MRI*, Inverse Problems, 30 (2014), https://doi.org/10.1088/0266-5611/30/5/055012.

[13] Z. Wang, A. C. Bovik, H. R. Sheikh, and E. P. Simoncelli, *Image quality assessment: From error visibility to structural similarity*, IEEE Transactions on Image Processing, 13 (2004), pp. 600–612, https://doi.org/10.1109/TIP.2003.819861.